Lattice element method

Vincent Topin, Jean-Yves Delenne and Farhang Radjai

Laboratoire de Mécanique et Génie Civil, CNRS - Université Montpellier 2, Place Eugène Bataillon, 34095 Montpellier cedex 05

1 Introduction

For about thirty years, discrete element methods (DEM) of granular materials have been largely developed and they present today high potentiality both in academic research and for industrial applications. In most methods, the particle movements are computed by means the equations of dynamics and pair-wise contact interactions. They can easily be extended to account for cohesive interactions which are often simply supplemented to the repulsive elastic and frictional interactions of cohesionless materials. But, cohesive behavior may also arise from the action of a binding matrix partially filling the space between particles as in cemented granular materials. The effect of a binding matrix occurring in high volume fraction cannot be reduced to a pair-wise interaction law. A sub-particle discretization of both the particles and the matrix is therefore the only viable approach in this limit. We introduce here the lattice element method (LEM), which relies on 1D-element meshing of both the particles and binding matrix. Several simple rheological models can be used to describe the behavior of each phase. Moreover, the behavior of the different interfaces between the phases can be accounted for. In this way, the model gives access to the behavior and failure of cohesive bonds but also to that of particles and matrix. The LEM may be considered to be a generalization of DEM in which the discrete elements are the material points belonging to each phase instead of the particles as rigid bodies. We briefly present this approach in a 2D framework.

2 Network connectivity

The triangular lattice used for the discretization can either be regular or irregular. Each node has a fixed number of neighbors unlike in the DEM applied to the particles where we need to update frequently the neighborhood list.

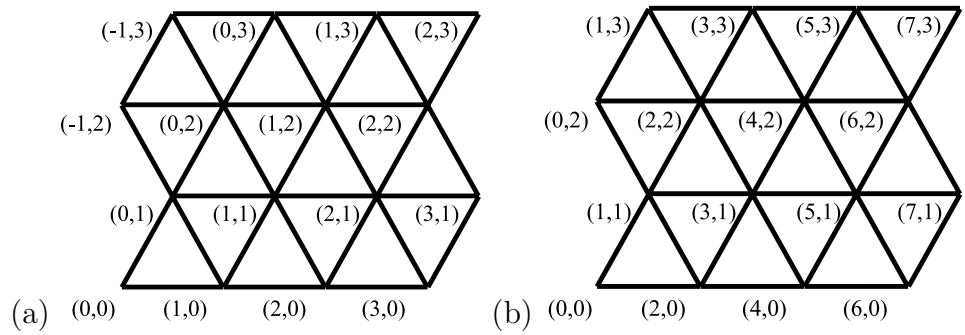

Fig. 1. Illustration of two methods for the indexing a lattice.

Another advantage of using a lattice with prescribed connectivity is the possibility of indexing the nodes whereby optimizing computation time.

Usually, the nodes of a lattice are described using the (k, l) coordinates of the lattice; figure 1a. A more efficient method is, however, to associate (k, l) to a column number and row as shown in figure 1b.

In a lattice with N_y lines each composed of N_x nodes, the total number of nodes N is given by:

$$N = N_x N_y - N_y/2 \tag{1}$$

and its dimensions (L_x, L_y) for elements of equilibrium length a are:

$$\begin{aligned} L_x &= N_x a \\ L_y &= \tfrac{\sqrt{3}}{2} N_y a \end{aligned} \tag{2}$$

The N nodes can be labeled using the pair (k, l) (figure 1 (a)) and the number of nodes per line N_x:

$$i = \frac{k + l(2N_x - 1)}{2} \tag{3}$$

This i index allows us to browse very easily the network. The index of each of the six neighbors of a node i can be obtained by adding or subtracting the number of nodes between them; figure 2a.

3 1D rheological elements

In the LEM, it is possible to assign different rheological behaviors to the lattice elements. In the simplest case, one can use "fuse" elements characterized only

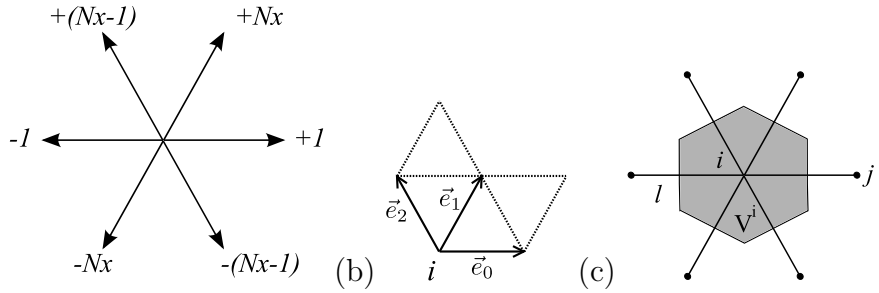

caption
(a) Indexing neighbors; (b) illustration of the three branches of the network; (c) unit cell on which the stress at node i is defined.

by a rupture threshold. This type of element has been used by many authors for the statistical analysis of failure (Herrmann and Roux [1990]). To account for the elastic behavior, two simple models of 1D elements are possible. The first model consists of spring element that transmit only radial forces between the lattice nodes [1] . For the second model, we use beam elements which can transmit shear and torque, as well.

3.1 Spring-like element

The 1D spring-like element has a simple elastic-fragile behavior. Using such elements one can reproduce macroscopic elastic-brittle behavior at the lattice scale. Each element is characterized by a stiffness k and a rupture force f_c. The radial force f is given by:

$$f = k\Delta l \tag{4}$$

where Δl is the spring extension. Beyond the rupture point f_c, the stiffness of the element becomes zero.

For a regular triangular lattice of identical elements, the macroscopic effective moduli of extension k_{eff} and shear μ_{eff} are functions of the stiffness k of the elements (Schwartz et al. [1985]):

$$k_{eff} = \frac{\sqrt{3}}{2}k \quad \text{et} \quad \mu_{eff} = \frac{\sqrt{3}}{4}k \tag{5}$$

Notice that in this case, Poisson's ratio is constant and thus independent of the stiffness k:

$$\nu = \frac{k_{eff} - \mu_{eff}}{k_{eff} + \mu_{eff}} = \frac{1}{3} \tag{6}$$

[1] The shear strength of the assembly is ensured by the nodes connectivity.

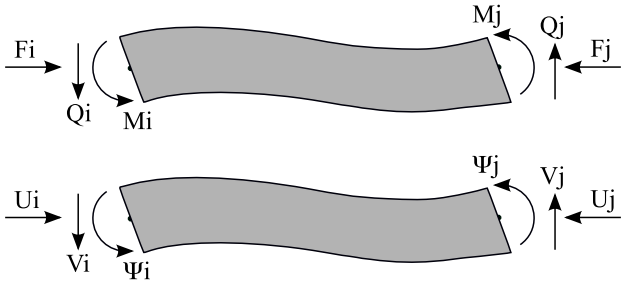

Fig. 2. Force and displacement at the nodes of a beam element.

3.2 Beam-like element

The use of 1D beam elements results in a more realistic macroscopic behavior. In this case, the elements can transmit a radial force F, a shearing force Q and a torque M (Schlangen and Garboczi [1996]) corresponding respectively to displacements U and V and rotation Ψ (Figure **??**):

The inter-node actions are given by the following relations:

$$F = \frac{EA}{l}(U_i - U_j) \tag{7}$$

$$Q = \frac{12EI}{l^3}(V_i - V_j) - \frac{6EI}{l^2}(\Psi_i - \Psi_j) \tag{8}$$

$$M = \frac{6EI}{l^2}(V_i - V_j) - \frac{4EI}{l}\left(\Psi_i - \frac{\Psi_j}{2}\right) \tag{9}$$

where E is Young's modulus, l is the length, I is the moment of inertia and A is the section area of the beam.

In the same way as for linear elastic elements, we can evaluate the effective moduli and Poisson's ratio of the lattice (Schlangen and Garboczi [1996]):

$$k_{eff} = \frac{\sqrt{3}}{2}\frac{EA}{l} \quad \text{et} \quad \mu_{eff} = \frac{\sqrt{3}}{4}\frac{EA}{l}\left(1 + \frac{12I}{Al^2}\right) \tag{10}$$

and

$$\nu = \frac{k_{eff} - \mu_{eff}}{k_{eff} + \mu_{eff}} = \left(\frac{1 - \frac{12I}{Al^2}}{3 + \frac{12I}{Al^2}}\right) - 1 < \frac{1}{3} \tag{11}$$

Notice that the use of beams is computationally more costly than linear springs. Moreover, in the case of samples with a large stiffness and disorder in failure thresholds, the difference of macroscopic behavior between the two models tends to decrease (Topin [2008]).

4 Numerical resolution

For the numerical resolution, the initial state is considered as the reference state. Forces and/or displacements can be applied to the boundary of the numerical sample. We assume that the displacements are small compared to the initial length of the elements. Different algorithms can be used to determine the equilibrium position of all nodes, e.g. by assigning a mass to the nodes one can use dynamic algorithms as in DEM.

In this section, an alternative quasistatic approach is presented. This approach is based on a minimization of the total potential energy of the system. The minimization is achieved through a conjugate gradient algorithm which has the advantage of being stable and fast. The first resolution step is to calculate the total potential energy of the system and its gradient. The sum of the energies is calculated along the three axes ($\vec{e_0}$,$\vec{e_1}$,$\vec{e_2}$) of the lattice using i index, see figure 2b. In the following, we consider both cases of spring and beam elements.

4.1 Spring elements

The degrees of freedom of the system are the node displacements $\vec{r_i}$. Denoting the initial position by $\vec{R_i}$, the relative displacements are:

$$\vec{\Delta}_i = \vec{r_i} - \vec{R_i} \tag{12}$$

At equilibrium, we define the square distance l_{ij}^2 between a node i and its neighbor j:

$$l_{ij}^2 + q_{ij} \equiv (\vec{r_j} - \vec{r_i})^2 = (\Delta x_j - \Delta x_i + l x_{ij})^2 + (\Delta y_j - \Delta y_i + l y_{ij})^2 \tag{13}$$

with $\Delta_{ix} \equiv \vec{\Delta}_i.\vec{e}_x$, $\Delta_{iy} \equiv \vec{\Delta}^{k,l}.\vec{e}_y$ and where $\sqrt{l_{ij}^2 + q_{ij}}$ is the Euclidean distance between i and j.

To simplify the notations, we consider the case of an element between two nodes i and j. For a linear elastic stiffness k undergoing an extension Δl, the elastic energy U is:

$$U = \frac{1}{2} k \Delta l^2 \tag{14}$$

The potential energy is given by:

$$U_{ij} = \tfrac{1}{2} k \left(\sqrt{l^2 + q} - l \right)^2 \tag{15}$$

The gradient of energy in the orthonormal global frame $(0, x, y)$ is given by:

$$\vec{\nabla} U_{ij} = \begin{pmatrix} \delta U_{ij}/\delta x \\ \delta U_{ij}/\delta y \end{pmatrix} \tag{16}$$

The new equilibrium can then be determined by minimizing the total potential energy:

$$U_{tot} = \sum_{i,j,} U_{ij} \tag{17}$$

4.2 Beam element

The potential energy U of a beam is given by the energies associated with radial F and transverse Q forces and momentum M (Timoshenko [1968]):

$$U = U_F + U_Q + U_M = \frac{1}{2} \int_0^l \left(\frac{F^2}{AE} + \frac{Q^2}{k_c GA} + \frac{M^2}{EI} \right) dx \tag{18}$$

where $G = E/2(1+\nu)$ is the shear modulus, ν the Poisson ratio of the beam and $k_c = (10+10\nu)/(12+11\nu)$ the Timoshenko's coefficient of transverse shear modified by (Cowper [1966]) for a beam of rectangular section.

Assuming that F, Q and M are constant and do not depend on the longitudinal axis x, we have:

$$U_F = \frac{F^2}{2AE} l \ , \ U_Q = \frac{Q^2}{2k_c GA} l \ \text{ and } U_M = \frac{M^2}{2EI} l \tag{19}$$

We define the axial $\Delta l = U_i - U_j$ and transversal $\Delta h = V_i - V_j$ extensions as well as the angular variations $\Delta\Psi = \Psi_i - \Psi_j$ and $\Delta\Psi_2 = \Psi_i - \Psi_j/2$ from the node displacements.

For beams of square section of thickness b, we introduce a coefficient C_r defined as the ratio of the beam's thickness to its length:

$$C_r = \frac{b}{l} \ \text{ et } \ C_r^2 = \frac{A}{l^2} \tag{20}$$

Thus, the potential energy of a beam element can be written as the sum of the three following terms:

$$U_F = \frac{1}{2} E l C_r^2 \Delta l^2 \tag{21}$$

$$U_Q = \frac{(12+11\nu) E C_r^6 l^3}{40} \left(\frac{2}{l} \Delta h - \Delta \Psi \right)^2 \tag{22}$$

$$U_M = \frac{E C_r^4 l^3}{6} \left(\frac{3}{l} \Delta h - 2\Delta \Psi_2 \right)^2 \tag{23}$$

In the cylindrical global frame $(0, x, y, \phi)$, the gradient is given by:

$$\vec{\nabla} U_{ij} = \begin{pmatrix} \delta U_{ij}/\delta x \\ \delta U_{ij}/\delta y \\ \delta U_{ij}/\delta \phi \end{pmatrix} \tag{24}$$

From these equations we obtain the total potential energy of the system by summing all the potential energies of different elements.

4.3 Failure

An advantage of the LEM is to allow for the computation of the crack path in a simple way. Indeed, cracking is directly implemented at the level of the elements through a rupture threshold. Consider, for example, a failure criterion based on the radial force F. During the simulation, for each strain step, the radial forces are calculated in all elements after balancing the system (by minimizing the potential energy). In principle, the strain step should be small enough so that only one element will reach its threshold at a time ($F > F_c$). Since this would require very small strain increments, one of the following techniques can be used instead:

- when there are several critical elements with $F > F_c$, only the most critical element (with the largest force) is broken,
- All elements exceeding the force threshold F_c are broken.

To reduce the computation time, the second choice is more relevant. However, relaxation cycles should be performed at each increment to reach equilibrium before applying the next load increment. These relaxation cycles allow for the propagation of a crack within a single strain step. This physically corresponds to instantaneous propagation of cracks at imposed strain rate.

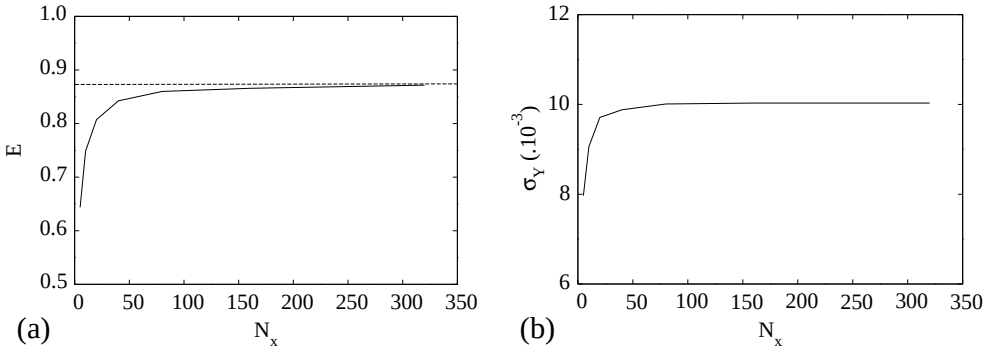

Fig. 3. Young modulus (a) and failure stress (b) as a function of the size N_x of sample.

5 Influence of meshing

We study here the influence of the mesh on the Young modulus and tensile strength of the lattice. This influence affects not only the number of cells that are involved in the simulation but also the geometrical disorder and stiffness introduced at the level of the elements.

5.1 Finite size effects

Figure 3 shows the Young modulus E and the failure stress σ_Y of a homogeneous square sample ($N_x = N_y$) loaded in uniaxial tension as a function of sample size. We use a regular triangular lattice of spring elements (stiffness $k = 1$, initial length $l = 1$).

We see that E and σ_Y rapidly converge to a constant. This value equals to $\sqrt{3}/2$ for the Young modulus. The failure threshold σ_Y is well defined for $N_x > 50$. In practice, for a system composed of many particles, it is therefore necessary to use approximately $50^2 = 2500$ nodes in each particle.

5.2 Disordered mesh

There are several ways of introducing disorder in a lattice model. The simplest technique is to produce an irregular network by applying a random deviation over all positions of nodes, see figure 4. Figure 6 shows the fracture surface of a two notched sample subjected to uniaxial tension for both regular (a) and irregular (b) meshing. It is clear that the crack propagate along the lattice network in the case of regular triangular mesh. Conversely, for an irregular mesh the curved shape of the two cracks shows that the disorder has erased the geometric bias.

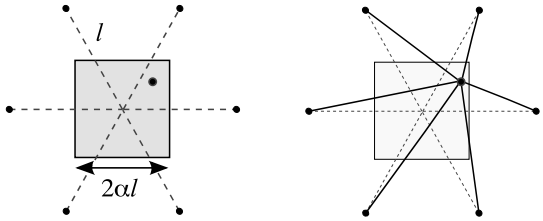

Fig. 4. Irregular mesh obtained by applying a random deviation to the nodes.

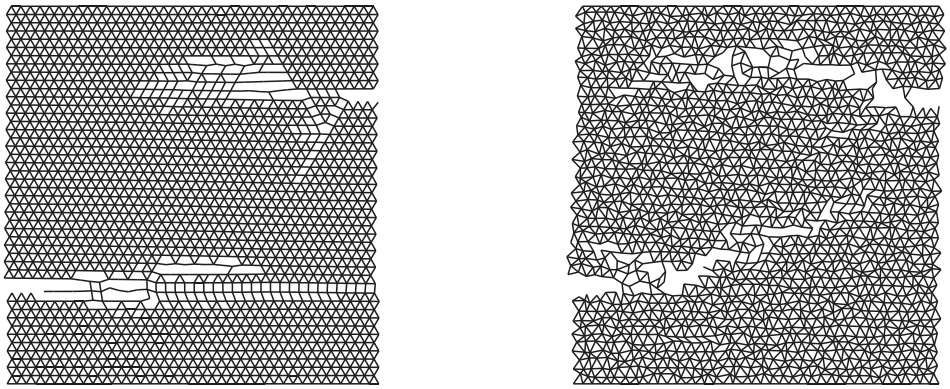

Fig. 5. Fracture of a notched homogeneous sample subjected to a tensile test with (a) regular meshing (b) irregular meshing.

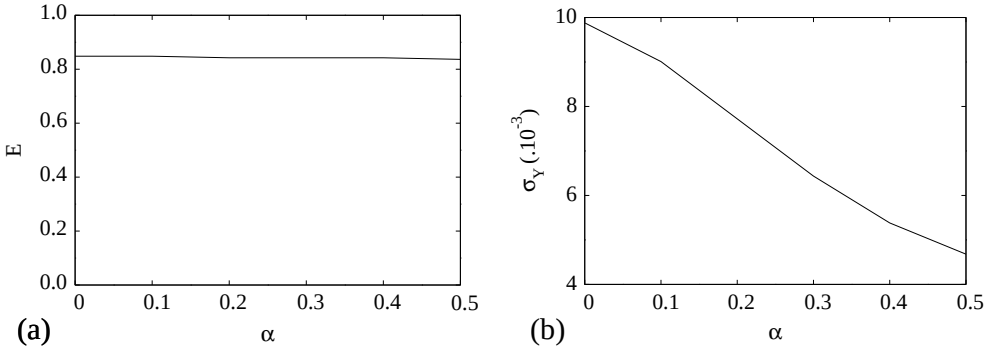

Fig. 6. Young modulus (a) and failure stress (b) as a function of the disorder parameter α.

Figure 6 shows the evolution of E and σ_Y as a function of the disorder parameter parameter !disorder α for a homogeneous sample loaded in tension. When $\alpha = 0$, the system is regular. For $\alpha = 0.5$, the node is randomly placed in a square of side $2\alpha = l$; figure 4. Notice that α has no influence on the Young modulus. However, the tensile strength decreases linearly with α. Thus, in the limiting case where $\alpha = 0.5$, σ_Y is divided by two. The Young modulus depends on the entire meshing. However, the tensile strength is related to the stress distribution which depends on disorder. Hence, the premature rupture of a single element can initiate a crack that may extend to the entire sample. A very irregular mesh may have elements that can cause premature cracking.

It is also possible to disorder the lattice by randomly removing a fraction β of elements. To avoid crystalline order, β should be larger than 0.15. However, as shown on the plots 7a and 7b, this method disturbs both the Young modulus and tensile strength.

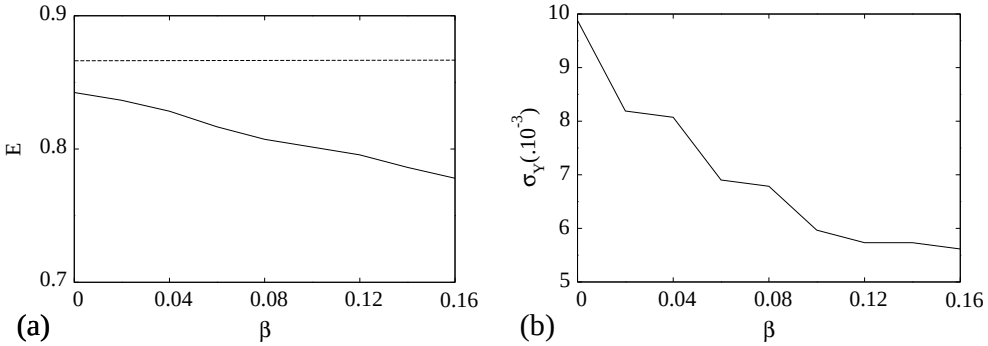

Fig. 7. Young modulus (a) and failure stress (b) versus the fraction β of removed links.

5.3 Granular disorder

At the mesoscopic scale, we can have a natural disorder related to the mechanical properties of different phases. In a cemented granular material, the particles often have a larger stiffness than the matrix. Figure 8 shows the fracture surface of a medium with inclusions of higher stiffness than that of the matrix under the same conditions as the test shown in figure 5. We notice that the cracking paths differ very little between regular and irregular meshes. In the regular case, the presence of particles is sufficient to produce the necessary disorder for a homogeneous behavior.

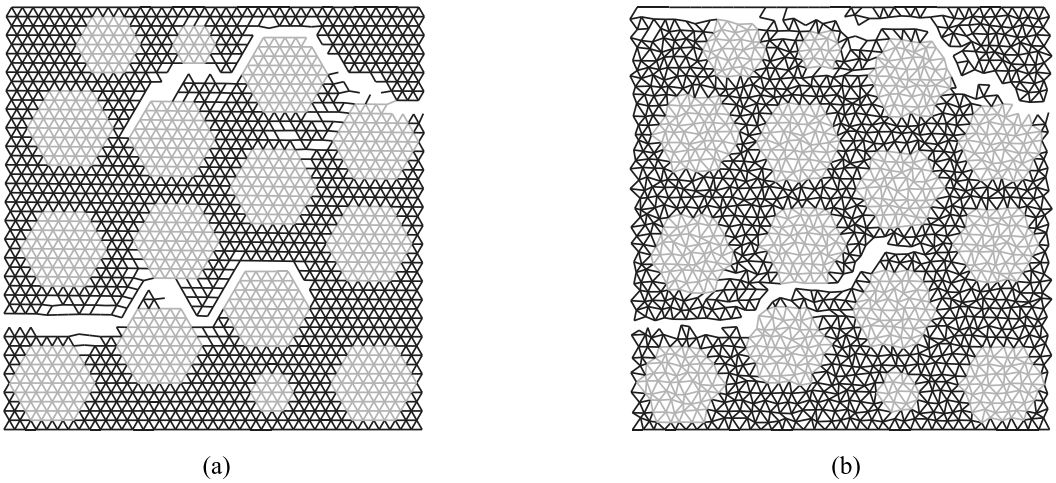

Fig. 8. Fracture patterns of a notched heterogeneous sample subjected to tensile test: (a) regular mesh (b) irregular mesh.

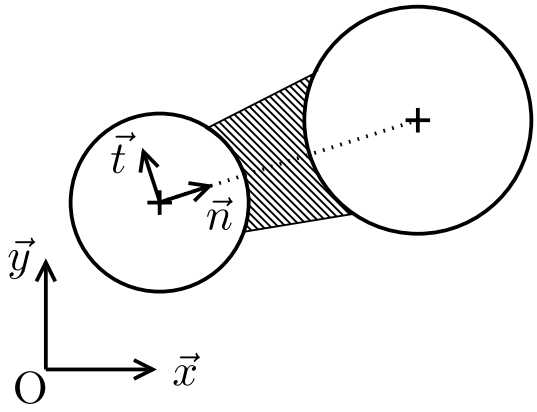

Fig. 9. A pair of particles in the global coordinate system.

6 Comparison between LEM and cohesive DEM

DEM with cohesive interactions is based on the assumption that the particles are rigid discrete elements. In this method, we cannot determine the stress distribution at a sub-particle scale and only the contact forces between particles can be calculated. On the contrary, the LEM allows one to access the stresses in each phase of the medium. In order to calculate the contact forces, only the binder phase between two particles are considered: particle-particle interfaces and the phase matrix. The stress tensor $\vec{\sigma}$ in a phase between a pair of particles is obtained from the calculated stresses at the nodes in the bulk of that phase.

We denote by $\vec{n}$ and $\vec{t}$ the normal and tangential unit vectors associated with the two particles (figure 9), the normal and tangential forces $\vec{f_n}$ and $\vec{f_t}$, respectively, are given by:

$$\begin{aligned} \vec{f_n} &= \vec{\sigma}.\vec{n}.\vec{n} \\ \vec{f_t} &= \vec{\sigma}.\vec{n}.\vec{t} \end{aligned} \tag{25}$$

Figure 10 displays the normal force networks in a bidisperse sample loaded in simple compression. The contact force distributions obtained by the LEM and DEM are very similar. We distinguish high vertical force chains (strong network) which cross mainly large particles. The network of weak forces is mainly localized at the contacts between small particles. The Pearson correlation coefficient between the two networks is 0.9.

In order to characterize the force heterogeneity, we compute the probability density function of contact forces for a low matrix volume fraction. The studied sample consists of about 5000 particles, corresponding to a LEM mesh of nearly 1 million elements. The mechanical properties attributed to each phase

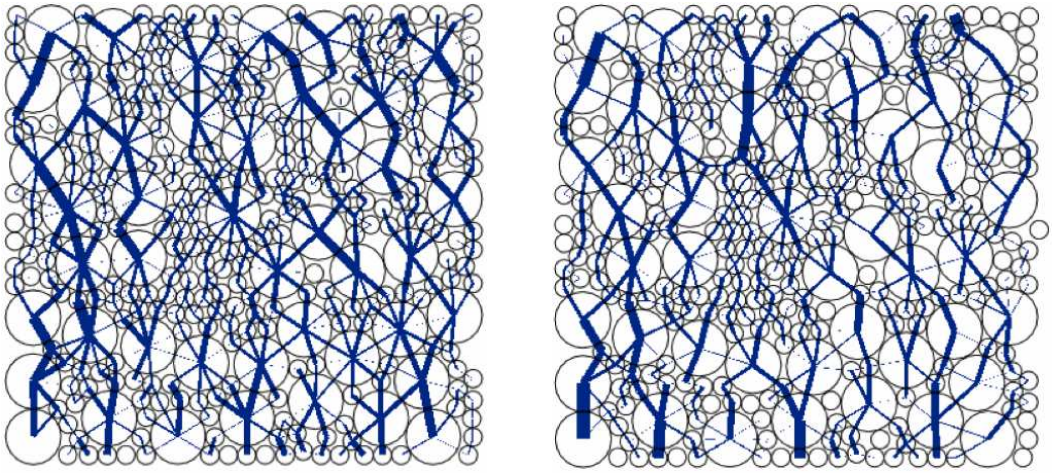

Fig. 10. Normal force networks computed by (a) LEM and (b) DEM with cohesion.

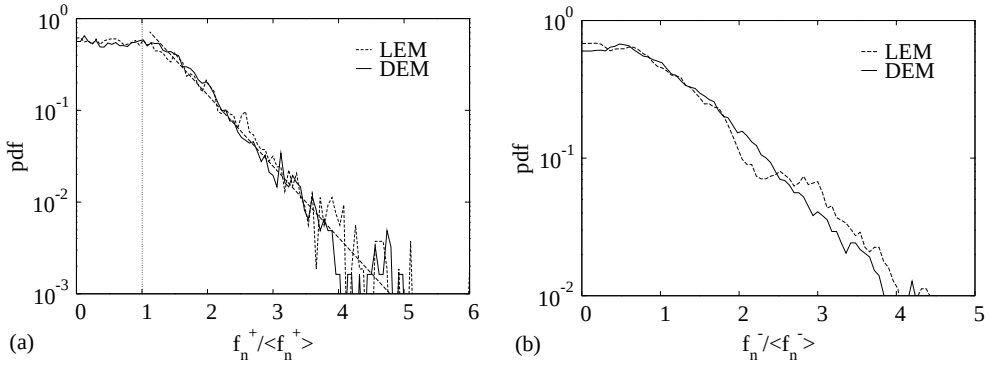

Fig. 11. Probability densities of normal forces (a) in compression and (b) in tension.

are the same as in the previous study. The contact forces between the particles are directly calculated by the LEM method with a high adhesion between the particles. Contact forces in the LEM simulation are calculated by integrating the stresses on the contact area. The initial configuration is the same in both simulations and both samples are subjected to uniaxial compression.

Figures 11a and 11b show the probability densities of the normal contact forces in compression f_n^+ and in tension f_n^- for LEM and DEM. These distributions are very similar, indicating that for a low matrix content both methods are equivalent in terms of stress transmission.

In both compression and tension cases we distinguish two parts:

- an exponential part corresponding to the strong force network (forces above the mean force)
- a range corresponding to the weak network which exhibits an almost uniform distribution. These weak forces represent around 60% of the contacts and are a signature of the arching.

It is also noteworthy that the weak forces extend also to the tensile forces and that cohesion amplifies the arching.

Similar results were obtained for the tangential force distribution f_t (Topin et al. [2009]). Finally, we remark that this distribution is similar to that observed in the case of cohesionless granular materials (Radjai et al. [1998]). This is consistent with the fact that we consider here a granular material with a very small amount of binding matrix.

7 Alternative approaches to the LEM

There are two main alternatives to the LEM for modeling granular materials with a high cement content. The "beam-particle" model (D'Addetta et al. [2001, 2002]) can be seen as a hybrid approach between the DEM with cohesion and the LEM. In this method the beams connect the centers of particles through a network of beams that can transmit tensile actions as well as shear and rotation.

In 2D, for a beam placed between particles i and j we define:

$$a = \frac{l}{E_b A},\ b = \frac{l}{G_b A},\ c = \frac{l^3}{EI} \tag{26}$$

where E_b and G_b are the Young and shear modulus of the beam, A is the area of the cross section of the beam, I is bending moment of inertia. In the model, we have $b = 2$ (which corresponds to a Poisson's ratio $\nu_b = 0$). In the local frame of the beam, three degrees of freedom are assigned to each center connected to the particle beam. These degrees of freedom are, for node i: the displacement vector (u_x^i, u_y^i) and the rotation ψ. The beam's force acting on particle i is given by:

$$F_x^i = \alpha(u_x^j - u_x^i) \tag{27}$$

$$F_y^i = \beta(u_y^j - u_y^i) - \frac{\beta l}{2}(\Psi_i + \Psi_j) \tag{28}$$

$$M_z^i = \frac{\beta l}{2}(u_y^j - u_y^i - l\psi^j) - \delta l^2\,(\Psi_j - \Psi_i) \tag{29}$$

where $\alpha = 1/a$, $\beta = 1/(b + 1/12c)$ and $\delta = \beta(b/c + 1/3)$.

In this model, the failure is taken into account using the criterion:

$$p_b = \left(\frac{\epsilon_b}{\epsilon_{b,max}}\right)^2 + \frac{\max\left(|\psi_i|, |\psi_j|\right)}{\psi_{max}} \geq 1 \tag{30}$$

where $\epsilon_b = \frac{\Delta l}{l}$ is the longitudinal deformation of the beam and $\epsilon_{b,max}$ and ψ_{max} are the failure thresholds.

A second alternative model is to use a "cohesive zone" approach (Raous et al. [1999]) associated with a discrete element method (Pelissou et al. [2009]). In this approach, it is possible to integrate a complex behavior at interfaces between particles. A major drawback of this type of methods is that the computation time greatly depends on the number of cohesive zones taken into account and that these zones have predefined crack paths. Moreover, this method can not easily simulate the case of materials with strong gradients of properties.

References

G.R. Cowper. The shear coefficient in timoshenko's beam theory. *ASME Journal of Applied Mechanics*, 33:335–340, 1966.

G. A. D'Addetta, F. Kun, E. Ramm, and H. J. Herrmann. *Continuous and discontinuous modelling of cohesive frictional materials*, chapter From solids to granulates – Discrete element simulations of fracture and fragmentation processes in geomaterials, pages 231–258. Springer, 2001.

G. A. D'Addetta, F. Kun, and E. Ramm. On the application of a discrete model to the fracture process of cohesive granular materials. *Granular Matter*, 4:77–90, 2002.

H. J. Herrmann and S. Roux, editors. *Statistical Models for Fracture in Disordered Media*. North Holland, Amsterdam, 1990.

C. Pelissou, J. Baccou, Y. Monerie, and F. Perales. Determination of the size of the representative volume element for random quasi-brittle composites. *International Journal of Solids and Structures*, 46(14-15):2842–2855, 2009.

F. Radjai, D. E. Wolf, M. Jean, and J. J. Moreau. Bimodal character of stress transmission in granular packings. *Phys. Rev. Lett.*, 80(1):61–64, 1998.

M. Raous, L. Cangémi, and M. Cocu. A consistent model coupling adhesion, friction, and unilateral contact. *Computer Methods in Applied Mechanics and Engineering*, 177(3-4):383–399, 1999.

E. Schlangen and E. J. Garboczi. New method for simulating fracture using an elastically uniform random geometry lattice. *International Journal of Engineering Science*, 34(10):1131–1144, 1996.

Lawrence M. Schwartz, Shechao Feng, M. F. Thorpe, and Pabitra N. Sen.

Behavior of depleted elastic networks: Comparison of effective-medium and numerical calculations. *Phys. Rev. B*, 32(7):4607–, 1985.

S.P. Timoshenko. *Résistance des matériaux*. Dunod, Paris, 1968.

V. Topin. *Matériaux granulaires cimentés : modélisation et application á l'albumen de blé*. PhD thesis, Université Montpellier 2, 2008.

V. Topin, F. Radjai, and J. Y. Delenne. Subparticle stress fields in granular solids. *Physical Review E*, 79(5), 2009.